METRICA
METRology Institutional CAtalog

ISTITUTO NAZIONALE DI RICERCA METROLOGICA
Repository Istituzionale

Enhanced Directional Light Emission Assisted by Resonant Bloch Surface Waves in Circular Cavities

This is the author's submitted version of the contribution published as:

Original
Enhanced Directional Light Emission Assisted by Resonant Bloch Surface Waves in Circular Cavities / Stella, U.; Boarino, L.; De Leo, N.; Munzert, P.; Descrovi, E.. - In: ACS PHOTONICS. - ISSN 2330-4022. - 6:8(2019), pp. 2073-2082. [10.1021/acsphotonics.9b00570]

Availability:
This version is available at: 11696/61216 since: 2020-02-10T18:27:56Z

Publisher:
American Chemical Society

Published
DOI:10.1021/acsphotonics.9b00570

Terms of use:

This article is made available under terms and conditions as specified in the corresponding bibliographic description in the repository

Publisher copyright
American Chemical Society (ACS)
Copyright © American Chemical Society after peer review and after technical editing by the publisher. To access the final edited and published work see the DOI above.

(Article begins on next page)

19 April 2024

Enhanced directional light emission assisted by resonant Bloch Surface Waves in circular cavities

Ugo Stella[1], Luca Boarino[2], Natascia De Leo[2], Peter Munzert[2], and Emiliano Descrovi[1]*

[1] Department of Applied Science and Technology (DISAT), Politecnico di Torino, C.so Duca degli Abruzzi 24, Torino, IT-10129, Italy.

[2] Quantum Research Labs & Nanofacility Piemonte, Nanoscience & Materials Division, Istituto Nazionale di Ricerca Metrologica, Strada delle Cacce 91, Torino, IT-10135, Italy.

[3] Fraunhofer Institute for Applied Optics and Precision Engineering IOF, Albert-Einstein-Str. 7, Jena DE-07745, Germany

Corresponding Author:

Emiliano Descrovi: emiliano.descrovi@polito.it

Phone: +39 011 090 7352

ABSTRACT: The management of spontaneous light emission at the nanoscale is a crucial aspect in many application domains dealing with lighting, optical communications and quantum information systems. Two widespread approaches to target this topic are based on plasmonic structures and dielectric photonic crystals, which have demonstrated a high potential in controlling spectral, angular and temporal features of the emission. Both approaches exhibit rather complementary advantages, and many efforts are nowadays undertaken to find hybrid solutions taking the best from the two sides. In his framework, we propose a photonic device based on a dielectric multilayer, which is shown to control the spontaneous emission from organic dyes embedded therein. Such a result is achieved by exploiting the near-field interaction of emitters to Bloch Surface Waves resonantly coupled within a sub-wavelength cavity surrounded by a diffractive structure. A bright, monochromatic spontaneous emission is then obtained, with spectral width below 1 nm, a decay rate increased by a factor spanning from 16 to 33, and a propagation divergence below 5 degrees in free space. These findings are particularly promising for application in integrated photonic circuits and single-photon sources.

KEYWORDS: Surface Waves, Photonic Cavity, Purcell effect, Directional Emission

INTRODUCTION

The control of spontaneous emission (SE) represents one of the most challenging topics for current research in nano-optics. According to the Fermi golden rule, the SE decay rate can be increased by properly engineering the Local Density of States (LDOS) associated to electromagnetic modes in dielectric or metallic micro and nanostructures. A common strategy to this end consists in confining light in space by providing resonators with small mode volumes (V) and high quality factors (Q) [1]. In previous works, dielectric 2D and 3D photonic crystals (PC) [2-5], patterned waveguides [6,7], nanowires [8-10], plasmonic antennas [11-13], plasmonic cavities [14-16], metamaterials [17-21] and other metallo-dielectric stacks [22], have been proposed wherein SE from integrated sources is found to be significantly increased. In order to reach higher Purcell factors for SE, the emitters have to be located in close proximity of the LDOS local maxima [23]. In dielectric PCs this might be difficult to attain, as photonic modes are preferentially confined within high-index regions of the structure [5], with only evanescent tails leaking in the surrounding medium. In plasmonic resonators, although high LDOS can be produced at dielectric/metallic interfaces, a main limitation is found in the strong absorption at visible wavelengths [24]. When dealing with nano-resonators, a general issue is represented by the typically low directionality of the power radiated in free space. Although individual objects such as metallic resonant nanostructures [11,12] can be designed to shape their angular radiative pattern, an accurate control on the coupled-emission direction can be achieved by employing more spatially extended [25,26] or periodic structures [27,29].

Here we propose an original concept for enhancing the radiative decay rate and directing the emission of organic dyes located on the surface of a patterned dielectric multilayer stack. The multilayer supports Bloch Surface Waves (BSW), which are exploited as a mean to resonantly transfer energy from emitters to free-space, through a resonant coupling effect. Although experimentally observed in the late 70s [30], BSW have recently gained a renewed interest [31] because of the opportunities they offer in flat photonics at visible, near- and mid-infrared frequencies [32-44], as complementary to Surface Plasmon Polaritons (SPP). With this respect, BSW feature a lower absorption, narrower mode resonances, longer propagation lengths, spectral and polarization tenability, as compared to SPP. The high energy confinement of BSW on top of the multilayer [45] can be particularly advantageous to exploit coupling effects involving nano-sources or absorbers deposited on the surface [46-53], for example in sensing applications [54,55]. In the present case, BSW are exploited for a twofold goal, namely to enhance the decay rate of fluorescent molecules within a surface cavity and to deliver the radiated coupled power away from the cavity region, toward a diffractive element for further free-space out-coupling.

RESULTS AND DISCUSSION

A schematic of the proposed device is illustrated in Figure 1a. A dielectric multilayered structure (also referred to as a one-dimensional photonic crystal, 1DPC) constituted by a stack sequence of Silica and Tantalia slabs is deposited on a thin glass substrate, as detailed in the Methods section. The multilayer supports TE-polarized Bloch Surface Waves (BSW) localized at the top interface, at wavelengths below 600 nm. BSWs are tightly bound to the surface and can propagate for several hundreds of microns, as the number of stack layers is large enough to reduce significantly losses due to radiation leakage through the glass substrate [56]. On the multilayer surface, a 75 nm-thick layer of dye-doped PMMA is spun, then patterned with concentric rings. The deposition of the PMMA layer redshifts the BSW dispersion curve by virtue of the well-known dielectric loading effect [32]. The pattern includes an inner region associated to a circular cavity and an outer region corresponding to a circular grating outcoupler. The cavity is constituted by a central spacer surrounded by a series of periodic corrugations acting as a Distributed Bragg Reflector (DBR) for BSWs in a specific spectral range.

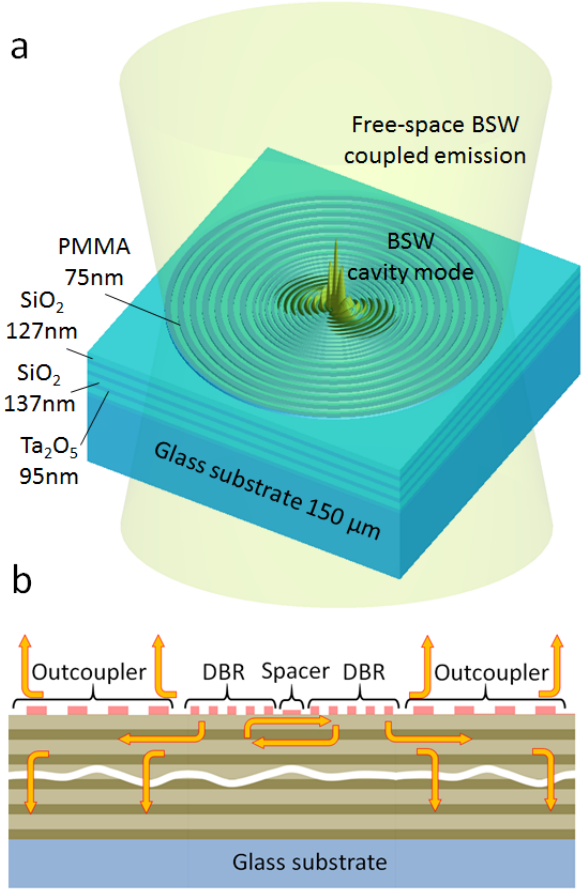

Figure 1. a) Sketch of the device showing the dielectric multilayer topped by a patterned dye-doped PMMA layer. The circular cavity and the grating outcoupler are etched in the PMMA layer. b) Working principle of the device showing the mechanism of emission coupling to the BSW cavity mode and corresponding diffraction by means of the outcoupler.

In the framework of two-dimensional optics [57], this structure represents an example of a circular Fabry-Pérot cavity for BSW [58], additionally provided with an external diffractive light outcoupler (Figure 1b). The organic dyes embedded within the PMMA spacer volume are excited by a tightly focused pulsed laser beam (see Methods section). A portion of the emitted fluorescence couples to the BSW cavity mode, depending on the randomly distributed orientations and positions of the dye molecules in PMMA [47]. The cavity is circular in order to maximize the likelihood of the emitters to couple to the BSW cavity mode, which has an in-plane electric field associated thereto. Since the DBR has a finite number of periods, such a BSW-coupled fluorescence can tunnel through the DBR annular region, thus reaching the outcoupler and being diffracted out–of-plane in both air and glass. The outcoupler period is designed to diffract BSW-coupled fluorescence at the -1st order, along a direction perpendicular to the sample surface.

Bloch Surface Waves subwavelength cavities

As for Surface Plasmon Polaritons [14], periodic surface relieves can operate as DBRs for BSW, thus opening frequency gaps in the dispersion curve, wherein the mode propagation is forbidden [59]. We set up a 2D computational model of the Silica-Tantalia 1DPC terminated with a binary DBR inscribed in the 75-thick PMMA layer (Figure 2a). BSWs at different wavelengths are launched over a flat region of the 1DPC and then propagated towards the DBR (see Methods section). Depending on the grating period, BSWs can be partially transmitted or reflected. At each wavelength, the normalized power delivered by back-reflected BSWs is collected and used to calculate the spectrally-resolved reflectivity map shown in Figure 2a. The spectral width of the stop-band is generally determined by the effective refractive index contrast Δn_{eff} introduced by the DBR. At λ_0=570 nm, a n_{eff} between 1.038 and 1.167, modulated with a spatial period Λ_{DBR} =260 nm produces a 30 nm wide stop-band in the wavelength range from 550 nm to 580 nm (Figure 2b). The stop band is designed to be roughly centered about the maximum emission wavelength of the dye embedded in PMMA.

According to the 2D model, the inner spacer can be sized such that one or more BSW cavity modes are allowed (Figure 2c). For diameters D ranging from 540 nm to 580 nm, the BSW cavity is single-mode, the mode spectral position being tunable within the DBR stop band. In an exemplary design with D=570 nm and Λ_{DBR} =260 nm, a cavity mode occurs at λ_0=570 nm, as shown by a reflectivity dip in the stop band reported in Figure 2d. Although simplified, this 2D approach is useful to define the cavity geometrical parameters. However, the calculation of the cavity Q-factor, the mode volume and the corresponding field distribution requires a more realistic 3D model. In order to deal with a circular geometry, a point-like oscillating electric dipole located in the spacer center is introduced as a light source. The dipole has its momentum oriented parallel to the surface, thus maximizing the

mode coupling to TE-polarized BSWs. For each emission wavelength, the corresponding near-field distribution $|E(x,y)|^2$ is calculated over a plane 10 nm above the PMMA surface (Figure 2d, inset) and integrated. The collected near-field spectrum is then used to evaluate the cavity quality factor, which is found to be $Q=\lambda_0/\Delta\lambda=1440$ for a cavity configuration having 30 DBR periods (Λ_{DBR}=260 nm) and spacer diameters D ranging from 550 nm and 570 nm.

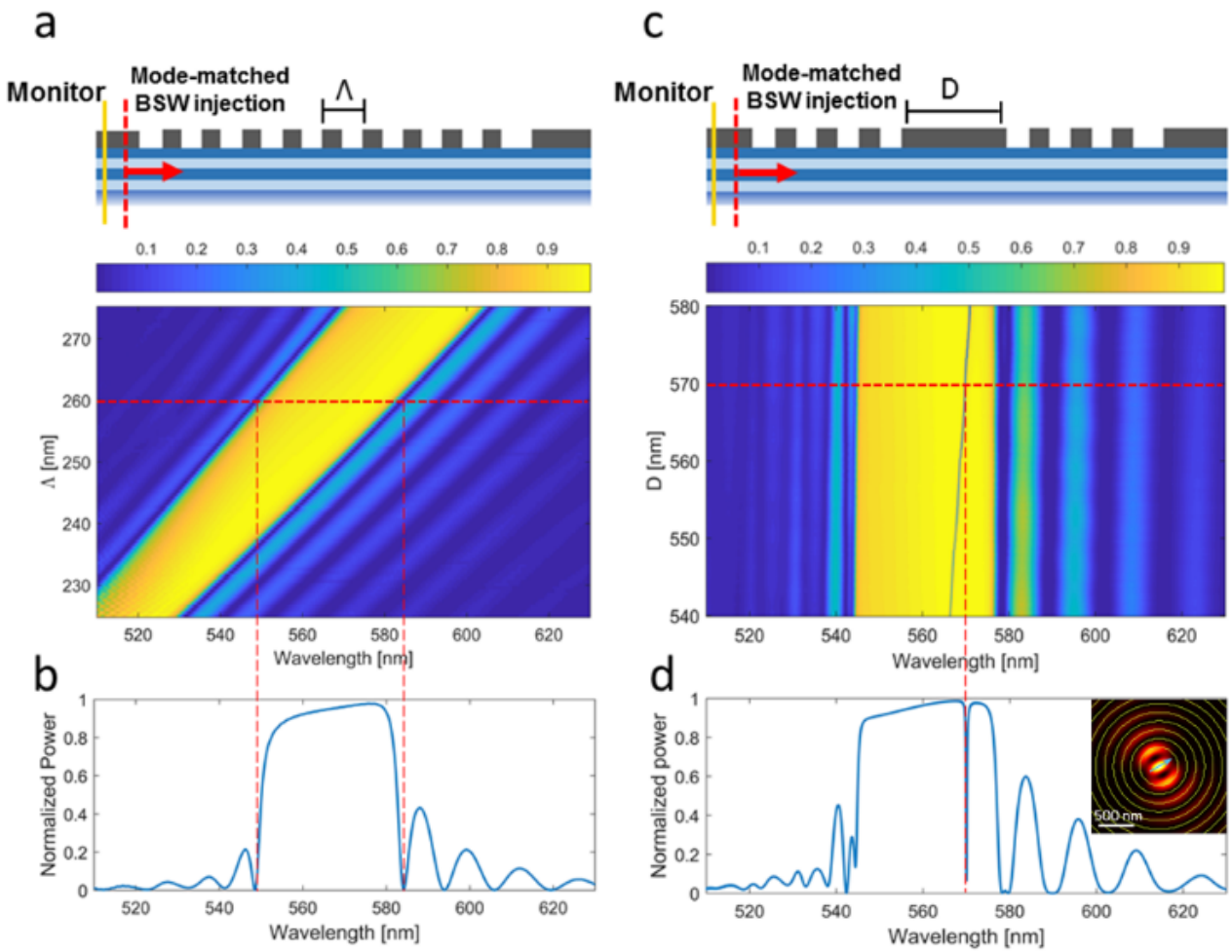

Figure 2. a) Sketch of the 2D model used to calculate the DBR period. A BSW mode is launched parallel to the multilayer surface, toward a grating inscribed in the PMMA film. The reflected power is collected by a monitor, located behind the BSW injection position. A dispersed, high-reflectivity spectral band appears for different corrugation periods. b) BSW reflectivity spectrum resulting from a grating period Λ_{DBR} =260 nm. The stop band is about 30 nm wide. c) Sketch of the two-dimensional model used to calculate the cavity spacer diameter. A weakly dispersed cavity mode appears for different spacer diameters. d) Exemplary cavity spectrum at λ_0=570 nm resulting from a spacer diameter D=570 nm. The cavity mode appears as a narrow reflectivity dip within the stop band. Inset: Intensity distribution $|E(x,y)|^2$ referred to the electromagnetic field emitted at λ_0 by a single dipole located in the cavity spacer, embedded 35 nm beneath the PMMA top surface. The dipole momentum is oriented as indicated by the cyan arrow.

Experimentally, dye molecules dispersed within the PMMA spacer are excited by a λ=505 nm pulsed laser beam. When the whole cavity is illuminated with a broad laser spot, a fluorescence image as shown in Figure 3a is observed. All excited dipoles radiate either in the free space or coupled to BSWs, according to the Local Density of States (LDOS) available at their specific locations. As the BSW-coupled radiation propagates along the structure surface, it gets weakly scattered by the structure relieves. The combination of the direct free-space emission and the BSW-coupled radiation scattering results in a broad fluorescence distribution that appears spatially homogeneous over the illuminated area. Part of the BSW-coupled fluorescence from dipoles spread all over the illuminated structure resonates within the cavity and gets scattered at the spacer, as indicated by the bright spot located at the cavity center. Unfortunately, this fluorescence spot includes a large amount of radiation emitted by dipoles excited out of the spacer, which are insensitive to the cavity mode LDOS. In order to reduce the emission from dipoles out of the spacer, the laser excitation needs to be tightly focused in the cavity center (Figure 3b). After a proper spatial filtering by means of a diaphragm (see Methods section), the image of the very cavity center can be then collected for the spectral and temporal analysis.

The spectroscopic signature of a typical BSW cavity-coupled emission reveals a two-peak profile, as shown in Figure 3c. The two peaks are separated by roughly 1 nm and are well fitted by a pair of Lorentzian profiles centered at λ_1=564.3 nm and λ_2=565.1 nm, with Full Width Half Maximum $\Delta\lambda_1$=0.6 nm and $\Delta\lambda_2$=0.4 nm, respectively. We account these two peaks to a slight deviation of the cavity from a perfectly circular shape. This leads to the appearance of two distinct modes associated to two orthogonal directions parallel the major and the minor axis of a generally elliptical cavity outline. Corresponding estimations for the cavity quality factor result in Q_1=940.5 and Q_2=1413.

A time-resolved decay of a typical BSW cavity-coupled emission can be obtained upon integration of the detected fluorescence over the spectral region from 563 nm and 566 nm (Figure 3d). As widely recognized, a single exponential function is unsuitable to fit the detected temporal trace, because the collected fluorescence results from multiple independent emitters which are eventually cavity-coupled with different coupling strengths and corresponding decay rates, depending on their positions and orientations. A stretched exponential function is usually employed in these circumstances [7,13,60]. However, we take advantage here from a simplified fitting function such as $I(t) = A_{fast} \cdot \exp\left(-t\tau_{fast}^{-1}\right) + A_{slow} \cdot \exp(-t\tau_{slow}^{-1}) + bckg$, which substantially assumes the overall fluorescence signal as given by two independent contributions from coupled (fast) and uncoupled (slow) emitters, summed to a constant background level, experimentally estimated at dark. The fast component is found to decay according to a time constant τ_{fast}=80 ps ± 17 ps, whilst the slow component has a time constant τ_{slow}= 2.62 ns ± 0.27 ns. The two terms contribute almost equally to the overall

detected intensity, with normalized amplitudes $A_{fast}^{(N)} = \frac{A_{fast}}{A_{fast}+A_{slow}} = 0.46$ and $A_{slow}^{(N)} = \frac{A_{slow}}{A_{fast}+A_{slow}} = 0.54$, respectively. We observe that the slow component decays similarly to the non-resonant fluorescence emitted from outside the cavity, whose temporal trace is indeed well fitted by a single exponential with time constant τ_0=2.68 ns ± 0.09 ns. For this reason we infer the slowly decaying signal as substantially associated to the emission from dipoles in the spacer that are either position- or polarization-mismatched with respect to the BSW cavity mode. Keeping into account the fast decay component only, a Purcell factor can be calculated as $F_P = {}^{\tau_0}/_{\tau_{fast}} \cong 33.5 \pm 8.2$. From the measured Purcell and Q factors, the BSW cavity mode volumes can be deduced as $V_1^{meas} = \frac{Q_1}{F_P}\frac{3}{4\pi^2}\left(\frac{\lambda}{n}\right)^3 = (2.13 \pm 0.5)\left(\frac{\lambda}{n}\right)^3$ and $V_2^{meas} = \frac{Q_2}{F_P}\frac{3}{4\pi^2}\left(\frac{\lambda}{n}\right)^3 = (3.2 \pm 0.8)\left(\frac{\lambda}{n}\right)^3$, which are both in good agreement with the calculated value $V^{calc} = 2.23\left(\frac{\lambda}{n}\right)^3$ at λ_0=570 nm, based on the 3D model described above.

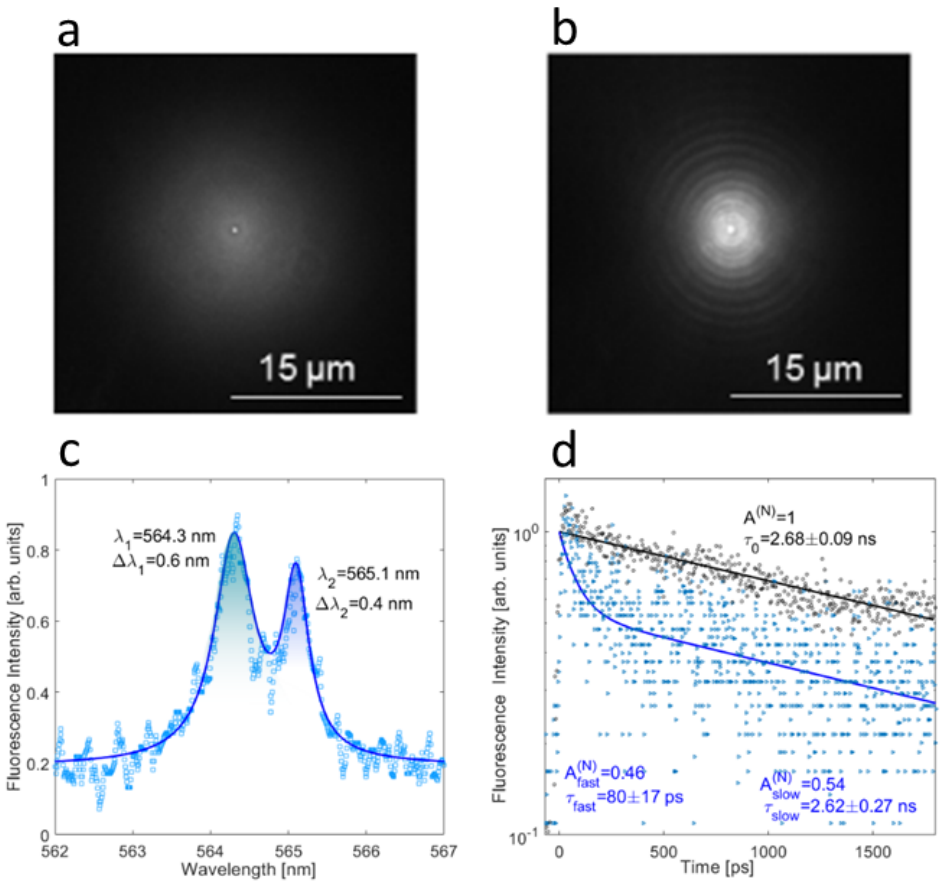

Figure 3. a) Fluorescence image of a BSW cavity (with no outcoupler) illuminated by a wide laser spot. b) Same cavity illuminated by a laser beam focused on the spacer. Fluorescence surrounding the central bright spot is associated to BSW cavity-coupled emission that is radially propagating and scattered by the DBR corrugations. c) Emission spectrum collected from direct-plane imaging of the

cavity center. d) Time-resolved decay of BSW cavity mode-coupled emission (blue triangles) and free-space emission from a flat 1DPC region (dark gray circles). The cavity-coupled signal is obtained by integrating the spectroscopic data over a 3 nm-wide spectral range, from 563 nm to 566 nm. Solid lines relate to corresponding exponential fitting functions.

Directional BSW cavity-coupled emission in free-space

Generally speaking, the BSW-coupled radiation occurs according to a well-defined dispersion curve. Upon application of the Bragg law, suitable diffraction gratings can be designed such that the BSW-coupled radiation in given spectral ranges is diffracted along specific directions [56,60]. In the following, we consider cavities having the BSW resonant mode peaked at λ_0=560 nm, surrounded by a circular diffractive element. In order to diffract BSW-coupled radiation at λ_0 normally to the multilayer surface, a circular grating outcoupler having period Λ_{DBR}=560 nm is introduced.

FDTD calculations are performed on a complete 3D model (including cavity and outcoupler). The source is represented by a single oscillating electric dipole buried in the center of the cavity spacer, with the dipole momentum lying parallel to the surface. Emission wavelength is λ_0=560 nm, thus matching the cavity mode. By far-field projecting the calculated near-field energy distribution around the structure, the angularly-resolved radiated power in the top and bottom half-spaces (air and glass, respectively) can be obtained. A normalization to the overall power emitted in a 4π solid angle is also performed. In Figures 4a,b, the integrated emitted power in air and glass within a NA=0.09 about the multilayer normal is plotted as a function of the number of outcoupler corrugation periods. Upon a comparison with two reference cases represented by a dipole within a flat 75 nm-thick PMMA slab on the multilayer and a dipole at a glass-air interface, we found that the presence of the outer grating greatly enhances the directionality of the emitted radiation from the dipole coupled to the BSW-cavity mode. Extraction performances increase with an increasing number of periods considered. As an example, for 30 outcoupler periods, the power collected within NA=0.09 in air is enhanced up to 26 and 62 times with respect to the dipole on a bare glass-air interface and on the flat multilayer, respectively. Similarly, in the glass medium, the diffracted BSW cavity-coupled power is 20 and 36 times larger as compared to the glass-air and the flat multilayer cases. These enhancement factors are merely due to an energy angular re-distribution and are not taking into account the Purcell factors previously discussed, as normalized powers are here concerned.

In order to appreciate the angular distribution of the emitted power, radiative patterns are calculated in the glass substrate for emitters in PMMA-topped flat 1DPC area and within the BSW cavity. In these calculations, multiple emitters are included, having random 3D orientations and emitting at λ_0=560 nm. Dipoles located over a flat 1DPC area radiate in free space, with some

coupling to leaky modes sustained by the multilayer. As a result, multiple rings beyond the critical angle are observed, as shown in Figure 4c. Experimental observations performed by means of Back Focal Plane (BFP) imaging (see Methods section) [56] are qualitatively in good agreement with the calculated pattern (Figure 4d). When the dipoles located in the cavity spacer are considered, a significant amount of power is beamed at emission angles close to the 1DPC surface normal (Figure 4e). This is expected, as the BSW cavity-coupled emission produced inside the cavity can tunnel through the DBR corrugations and then diffracted by the surrounding outcoupler. Experimentally, a similar BFP image is observed, as shown in Figure 4e, wherein the normally diffracted radiation intensity almost saturates the camera. The divergence of such a diffracted BSW-cavity mode-coupled fluorescence is well below NA=0.09, as indicated in the figure.

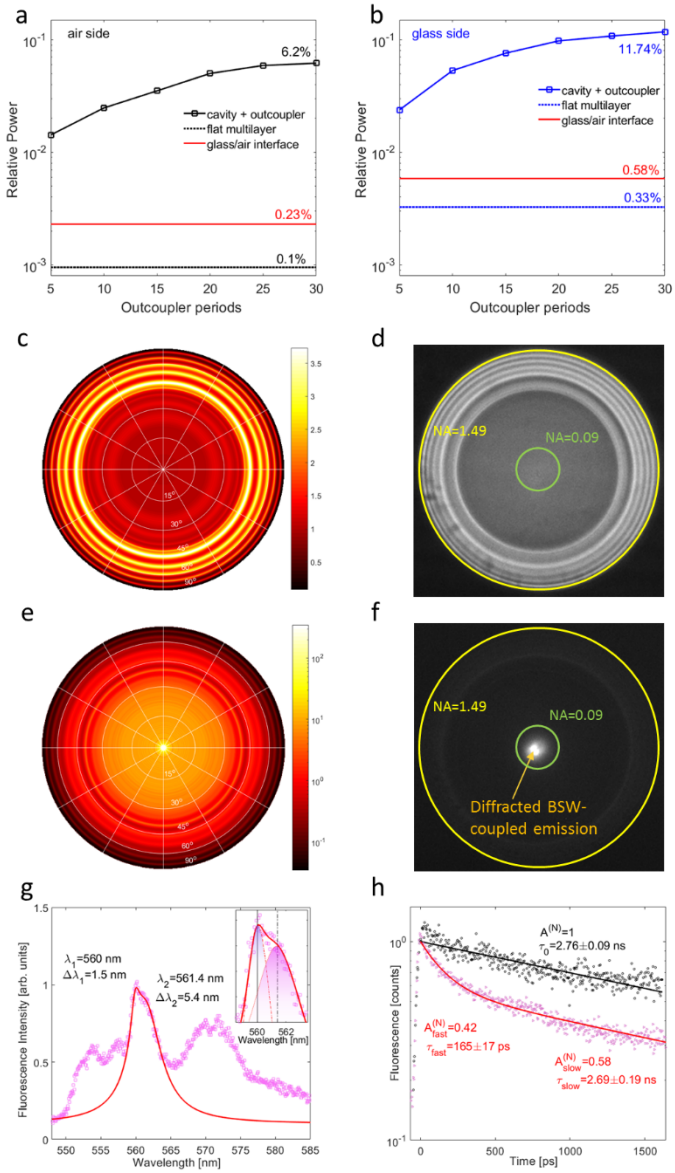

Figure 4. Calculated BSW cavity-coupled emission power from a single dipole located in the cavity spacer, diffracted within a NA=0.09 about the multilayer normal in air (a) and glass (b). For comparison purpose, single dipoles within a 75 nm-thick PMMA layer on top of a 1DPC and on a

bare glass-air interface are also considered. Power is normalized to the overall power emitted in a 4π solid angle. c) Calculated radiated intensity $|E(\theta,\phi)|^2$ in glass from multiple dipoles with 3D random orientations in a flat 75 nm-thick PMMA layer on 1DPC. Color scale is linear. Emission wavelength is λ=560 nm. d) Back Focal Plane image of fluorescence collected from a flat region of the PMMA-topped 1DPC by means of a NA=1.49 oil immersion objective. e) Calculated radiated intensity $|E(\theta,\phi)|^2$ in glass from multiple dipoles with random 3D orientations in the cavity spacer center. Color scale is logarithmic. Emission wavelength is λ=560 nm. f) Back Focal Plane image of fluorescence collected from cavity and outcoupler, wherein the cavity spacer only is illuminated by a tightly focused laser beam. g) Diffracted fluorescence spectrum collected at the central region of the BFP. The BSW cavity-coupled emission is well-fitted by a pair of Lorentzian functions. h) Time-resolved decay of fluorescence collected from the central region of the BFP for cavity and outcoupler (pink triangles) and for a flat 1DPC region (gray circles).

The BFP image can be spatially filtered by means of a diaphragm and then directed to the spectrometer entrance slit. In this way, only fluorescence diffracted at small angles about the optical axis is collected (see Methods section). The spectrometer slit aperture had to be kept as large as 200 μm and a 150 lines/mm grating is used in order to gather a signal high enough on the detector, at the expense of the spectral resolution attainable. As expected from design, a strong evidence of a BSW cavity-coupled fluorescence is observed (Figure 4e). A closer analysis reveals that the peak can be well-fitted by a pair of Lorentzian functions, spectrally separated by 1.4 nm. Similarly to the previous case, we account these two peaks to a slight asymmetry occurring during the cavity fabrication process. The higher background level observed is due to diffraction of emission contributions from cavity-mismatched dyes.

As temporal traces are concerned, fluorescence diffracted from a cavity+outcoupler system is observed to decay faster than the fluorescence from a flat sample area (Figure 4f). In analogy to the previous analysis, a two-exponential function is used for data fitting, resulting in a fast and a slow components with lifetime and relative amplitudes τ_{fast}=165 ps ±17 ps, $A_{fast}^{(N)} = \frac{A_{fast}}{A_{fast}+A_{slow}} = 0.42$ and τ_{slow}=2.69 ns ± 0.19 ns, $A_{slow}^{(N)} = \frac{A_{slow}}{A_{fast}+A_{slow}} = 0.58$, respectively. BFP fluorescence from a flat region decays exponentially with a time constant τ_0=2.76 ns ± 0.09 ns. By considering the fast component only, a corresponding Purcell factor can be calculated as $F_P = {}^{\tau_0}/_{\tau_{fast}} \cong 16.7 \pm 2.3$. Overall, the combination of the enhanced decay rate and the angular re-distribution of free-space radiation is expected to provide a final increase of power emitted within NA=0.09 and Δλ≈1 nm by

at least 400 times in air and 300 times in glass, as compared to the reference case wherein emitters are deposited on a bare glass-air interface.

CONCLUSIONS

A novel photonic structure is proposed, constituted by a dielectric multilayer patterned with an annular structure having an inner circular cavity and an outer diffraction grating. The overall structure supports a localized BSW resonant mode within the cavity and dispersed propagating BSW modes outside. Thanks to the availability of BSW modes, we managed to increase the decay rate of fluorescent emitters located in the cavity center and to diffract the corresponding coupled emission in free space with high control. The evidence of a fast decaying BSW cavity-coupled emission within NA=0.09 in the far field demonstrate the effectiveness of the mechanism proposed. It is observed, however, that the diffracted fluorescence presents a higher background level and a corresponding lower Purcell factor with respect to fluorescence directly imaged from the cavity center. We account this background as due to the overall fluorescent PMMA structure on top of the multilayer. In fact, despite the laser illumination is tightly focused, dye molecules spread all over the cavity are unavoidably excited and (at least, partially) coupled to propagating BSW that get ultimately diffracted. This effect is expected to reduce in case localized sources such as single quantum dots, diamond crystals or precisely defected 2D flakes are employed [62,63]. With this respect, our approach offers an advantage for emitters to be deposited and possibly manipulated directly on the structure surface, thus reducing fabrication efforts for source(s) integration.

METHODS

Sample fabrication. The 1DPC consists of a dielectric multilayer made of a stack of Ta2O5 (high refractive index) and SiO2 (low refractive index) layers, deposited on a glass coverslip (150 μm thickness) by plasma ion-assisted deposition under high vacuum conditions (APS904 coating system, Leybold Optics). The stack sequence is substrate-[Ta2O5-SiO2] x10-Ta2O5-SiO2-PMMA with a total of 23 layers, including PMMA. The Ta2O5 layer is 95 nm thick, the SiO2 layer is 137 nm thick. The top SiO2 layer on top of the stack is 127 nm thick. On top of the structure a 75 nm thick layer of dye-doped PMMA is spun for pattern fabrication. An organic dye, Atto-532 (fluorescence peak at λ_{Atto}=570 nm), is dissolved in PMMA before spinning, at a concentration of 0.01 mg/ml. Cavity and outcoupler structures are fabricated by electron beam lithography.

Time-resolved spectroscopic setup. The measurement apparatus can perform a spectral and temporal measurement of light emitted from the sample surface, with spatial and angular resolution. In Figure 5 a setup sketch is presented.

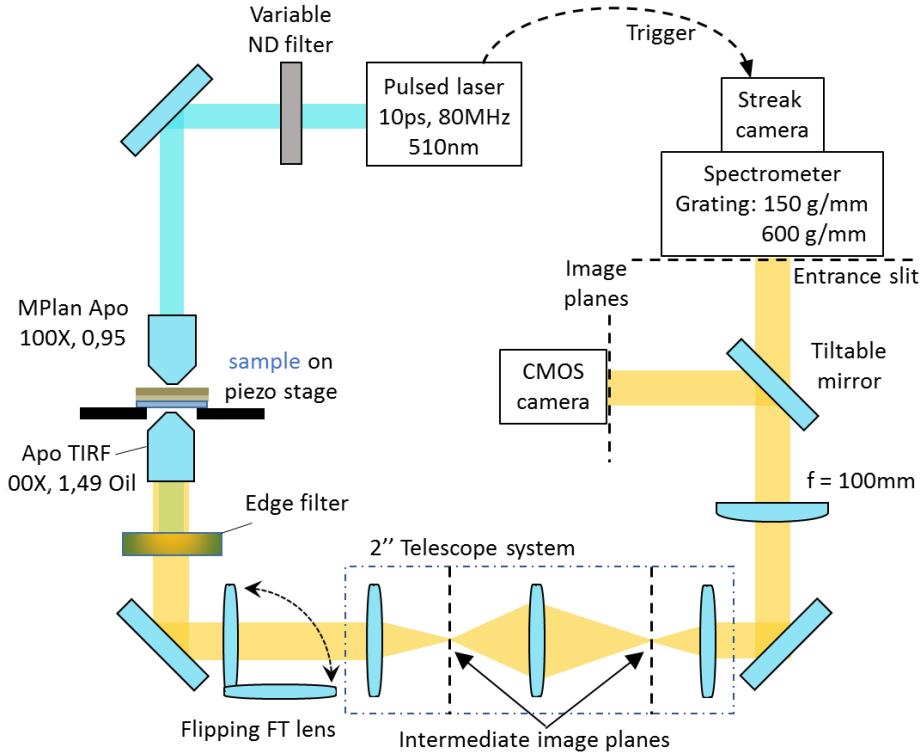

Figure 5. Optical setup for time-resolved spectral measurements with space/angular resolution capabilities. A flipping lens allows the imaging system to switch from a Back Focal Plane image or a direct-plane image detection. By properly employing masking elements (e.g. diaphragms or beam-blockers) on the two intermediate image planes, specific portions of either the direct-plane or the BFP images can be selectively projected on the spectrometer entrance slit.

The illumination is provided by means of an upper stage mounting a NA = 0.95 objective (Olympus MPlan Apo 100X) working in air and the collection is performed by a NA = 1.49 oil immersion objective (Nikon APO TIRF 1003). The illumination objective focuses a circularly polarized λ=505 nm pulsed laser (10 ps pulses, 80 MHz repetition rate, Tsunami, Spectra Physics) onto the sample, which is positioned on a 3-axis piezo stage (Physik Instrument). When measuring the decay rate of emitters coupled to the cavity mode, the excitation laser is accurately focused onto the spacer only, in order to minimize uncoupled emission radiated from other locations. Emitted fluorescence is collected by the oil immersion objective and then spectrally filtered (550 Long pass, Thorlabs) in order to block the laser radiation. A three-lens telescope system produces two intermediate image planes wherein spatial masks (e.g. a diaphragm or a beam blocker) can be inserted. The sample direct plane is then imaged either onto a CMOS camera (Thorlabs HR-CMOS DCC3260M) or on the entrance slit of a spectrometer (Acton SpectraPro 300, Princeton Instruments), thanks to a tiltable mirror. Only fluorescence emission coming from specific spatial regions defined according to the spatial masks can be then spectrally and temporally analyzed by the streak camera system

(Hamamatsu). Spectroscopic measurements related to direct-plane imaging mode are performed with a 600 lines/mm grating. In BFP imaging mode, the grating is changed to a 150 lines/mm, in order to increase the level of the detected signal, although at the expense of the spectral resolution. The time range of the streak camera is 2 ns, which is large enough to measure the uncoupled background Atto 532 lifetime. In front of the telescope system, a flipping lens performing Fourier Transformation is used to produce a Back Focal Plane (BFP) image of the collection objective onto the CMOS camera and/or the spectrometer entrance slit. By directing specific portions of the BFP image, only light propagating within corresponding angular ranges is spectrally and temporally analysed.

Numerical modeling. Numerical modeling is performed using the finite-difference time-domain method implemented in Lumerical software. First, a two-dimensional slice of the structure is used to compute the BSW modes supported by the 1DPC (topped with the PMMA layer). Next, BSW modes at specific wavelengths and effective refractive index are selected for injection into the simulation region, directed towards the corrugation acting as a Distributed Bragg Reflector. The reflected power is collected by the monitor.

Q-factor and Purcell factor are calculated based on a 3D model of the cavity, wherein single dipolar emitters are positioned within the cavity spacer. As the dipole-cavity coupling strength depends on the position and orientation of the dipole momentum with respect to the cavity geometry, the most favorable configuration has been considered, i.e. emitters are always located in the spacer center, 35 nm beneath the surface, with the dipole momentum oriented parallel to the surface. The Purcell factor is calculated as the power flow ratio from the emitter in the cavity and in a homogeneous medium (PMMA). The power flow is calculated by monitoring the energy dissipation rate of the emitter. In order to this, the simulation time window needs to be set large enough to guarantee a complete decay of the radiated electromagnetic energy, with a negligible residual within the simulation domain.

To cross-check the reliability of the numerical results, the Purcell factor is also estimated by calculating the quality factor Q and the mode volume V of the cavity at the resonance wavelength λ_{cavity} according to the well known formula $F_P = \frac{3}{4\pi^2}\left(\frac{\lambda}{n}\right)^3 \frac{Q}{V}$. The cavity mode volume can be estimated as $V = \frac{\int \varepsilon(\bar{r})|E(\bar{r})|^2 dV}{max\{\varepsilon(\bar{r})|E(\bar{r})|^2\}}$.

Angularly-resolved radiation patterns are calculated by projecting near-field power values collected by monitors surrounding the cavity and the outcouplers. Once the radiation intensity $|E(\theta,\phi)|^2$ is obtained, an integration in spherical coordinates is performed over proper angular integration intervals according to $\iint |E(\theta,\phi)|^2 \sin(\theta)\, d\theta d\phi$, leading to the emitted power values in the surrounding media.

ACKNOWLEDGMENTS

Dr. Angelo Angelini is acknowledged for fruitful scientific discussions and technical support in the early stage of the work. This research has received funding from the Italian Flagship Project NANOMAX (Progetto Bandiera MIUR PNR 2011–2013) and the European Commission through the project BILOBA (Grant agreement 318035).

REFERENCES

[1] Agio M, Cano DM. Nano-optics: the Purcell factor of nanoresonators. *Nature Photonics* 2013; 7(9): 674-675.

[2] Lodahl P, Van Driel AF, Nikolaev IS, Irman A, Overgaag K, Vanmaekelbergh DAM, Vos, WL. Controlling the dynamics of spontaneous emission from quantum dots by photonic crystals. *Nature* 2004; 430: 654-656.

[3] Kress A, Hofbauer F, Reinelt N, Krenner HJ, Meyer R, Boehm G, Finley JJ. Manipulation of the spontaneous emission dynamics of quantum dots in 2D photonic crystals. *Physical Review B* 2005; 71: 241304.

[4] Englund D, Fattal D, Waks E, Solomon G, Zhang B, Nakaoka T, Arakawa Y, Yamamoto Y, Vuckovic J. Controlling the spontaneous emission rate of single quantum dots in a two-dimensional photonic crystal. *Physical Review Letters* 2006; 95: 013904

[5] Noda S, Fujita M, Asano T. Spontaneous- emission control by photonic crystals and nanocavities. *Nature Photonics* 2007; 1: 449-458.

[6] Foresi JS, Villeneuve PR, Ferrera J, Thoen ER, Sternmeyer G, Fan S, Joannopoulos JD, Kimerling LC, Smith HI, Ippen EP. Photonic-bandgap microcavities in optical waveguides. *Nature* 1997; 390: 143-145.

[7] Yang Z, Pelton M, Bodnarchuk MI, Kovalenko MV, Waks E. Spontaneous emission enhancement of colloidal perovskite nanocrystals by a photonic crystal cavity. *Applied Physics Letters* 2017; 111: 221104.

[8] Caludon J, Bleuse J, Malik NS, Bazin M, Jaffrennou P, Gregersen N, Sauvan C, Lalanne P, Gérard JM. A highly efficient single-photon source based on a quantum dot in a photonic nanowire. *Nature Photonics* 2010; 4: 174-177.

[9] Bleuse J, Claudon J, Creasey M, Malik NS, Gérard JM, Maksymov I, Hugonin JP, Lelanne P. Inhibition, enhancement, and control of spontaneous emission in photonic nanowires. *Physical Review Letters* 2011; 106: 103601.

[10] Kolchin P, Pholchai N, Mikkelsen MH, Oh J, Ota S, Islam MS, Yin X, Zhang X. High purcell factor due to coupling of a single emitter to a dielectric slot waveguide. *Nano Letters* 2015;15: 464-468.

[11] Kinkhabwala A, Yu Z, Fan S, Avlasevich Y, Mullen K, Moerner WE. Large single-molecule fluorescence enhancements produced by a bowtie nanoantenna. *Nature Photon*ics 2009; 3 (11): 654–657.

[12] Belacel C, Habert B, Bigourdan F, Marquier F, Hugonin JP, Michaelis de Vasconcellos S, Lafosse X, Coolen L, Schwob C, Javaux C, Dubertret B, Greffet JJ, Senellart P, Maitre A. Controlling spontaneous emission with plasmonic optical patch antennas. *Nano Letters* 2013; 13 (4): 1516–1521.

[13] Akselrod GM, Argyropoulos C, Hoang TB, Ciracì C, Fang C, Huang J, Smith DR, Mikkelsen MH. Probing the mechanism of large Purcell enhancement in plasmonic nanoantennas. *Nature Photonics* 2014; 8: 835-840.

[14] Weeber JC, Bouhelier A, Colas des Francs G, Markey L, Dereux A. Submicrometer In-Plane Integrated Surface Plasmon Cavities. *Nano Letters* 2007; 7(5): 1352-1359.

[15] Russell KJ, Liu TL, Cui S, Hu EL. Large spontaneous emission enhancement in plasmonic nanocavities. *Nature Photonics* 2012; 6: 459-462.

[16] Derom S, Bouhelier A, Kumar A, Leray A, Weeber JC, Buil S, Quélin X, Hermier JP, Colas des Francs G. Single-molecule controlled emission in planar plasmonic cavities. *Physical Review B* 2014; 89(3):035401.

[17] Poddubny A, Iorsh I, Belov P, Kivshar Y. Hyperbolic metamaterials. *Nature Photonics* 2013; 7: 948-957.

[18] Li L, Wang W, Luk TS, Yang X, Gao J. Enhanced Quantum Dot Spontaneous Emission with Multilayer Metamaterial Nanostructures. *ACS Photonics* 2017; 4(3):501–508.

[19] Sreekanth, KV, Krishna KH, De Luca A, Strangi G. Large spontaneous emission rate enhancement in grating coupled hyperbolic metamaterials. *Scientific Rep*orts 2014; 4: 6340.

[20] Lu D, Kan JJ, Fullerton EE, Liu Z. Enhancing spontaneous emission rates of molecules using nanopatterned multilayer hyperbolic metamaterials. *Nature Nanotechnology* 2014; 9: 48–53.

[21] Ginzburg P, Roth DJ, Nasir ME, Segovia P, Krasavin AV, Levitt J, Hirvonen LM, Wells B, Suhling K, Richards D, Podolskiy V, Zayats AV. Spontaneous emission in non-local materials. *Light: science & applications* 2017; 6:e16273.

[22] Gubaydullin AR, Symonds C, Bellessa J, Ivanov KA, Kolykhalova ED, Sasin ME, Lemaitre A, Senellart P, Pozina G, Kaliteevski MA. Enhancement of spontaneous emission in Tamm plasmon structures. *Scientific Reports* 2017; 7: 9014.

[23] Barnes WL, Fluorescence near interfaces: the role of photonic mode density. *Journal of modern optics* 1998; 45(4): 661-699.

[24] Anger P, Bharadwaj P, Novotny L. Enhancement and Quenching of Single-Molecule fluorescence. *Physical Review Letters* 2006; 96: 113002.

[25] Ma Y, Ballesteros G, Zajac JM, Sun J, Gerardot BD. Highly directional emission from a quantum emitter embedded in a hemispherical cavity. *Optics Letters* 2015; 40:2373-6.

[26] Checcucci S, Lombardi P, Rizvi S, Sgrignuoli F, Gruhler N, Dieleman FBC, Cataliotti FS, Pernice WHP, Agio M, Toninelli C. Beaming light from a quantum emitter with a planar optical antenna. *Light: science & applications* 2017; 6: e16245.

[27] Davanço M, Rakher MT, Schuh D, Badolato A, Srinivasan K. A circular dielectric grating for vertical extraction of single quantum dot emission. *Applied Physics Letters* 2011; 99: 041102.

[28] Duong NMH, Xu ZQ, Kianinia M, Su R, Liu Z, Kim S, Bradac C, Tran TT, Wan Y, Li LJ, Solntsev A, Liu J, Aharonovich I.Enhanced Emission from WSe2 Monolayers Coupled to Circular Bragg Gratings. *ACS Photonics* 2018, 5(10):3950-3955.

[29] Newman WD, Cortes CL, Jacob Z. Enhanced and directional single-photon emission in hyperbolic metamaterials. *Journal of the Optical Society of America B* 2013; 30:766-775.

[30] Yeh P, Yariv A, Cho AY. Optical surface waves in periodic layered media. *Applied Physics Letters* 1978; 32: 104.

[31] Robertson WM, May MS. Surface electromagnetic wave excitation on one-dimensional photonic band-gap arrays. *Applied Physics Letters* 1999; 74: 1800.

[32] Descrovi E, Sfez T, Quaglio M, Brunazzo D, Dominici L, Michelotti F, Herzig HP, Martin OJF, Giorgis F. Guided Bloch surface waves on ultrathin polymeric ridges. *Nano Letters* 2010; 10(6): 2087-91.

[33] Sfez T, Descrovi E, Yu L, Quaglio M, Dominici L, Nakagawa W, Michelotti F, Giorgis F, Herzig HP. Bloch surface waves in ultrathin waveguides: near-field investigation of mode polarization and propagation. *Applied Physics Letters* 2010; 96: 151101.

[34] Ballarini M, Frascella F, Enrico E, Mandracci P, De Leo N, Michelotti F, Giorgis F, Descrovi E. Bloch surface waves-controlled fluorescence emission: Coupling into nanometer-sized polymeric waveguides. *Applied Physics Letters* 2012; 100: 063305.

[35] Liscidini M. Surface guided modes in photonic crystal ridges: the good, the bad, and the ugly. *Journal of the Optical Society of America B* 2012; 29: 2103-2109.

[36] Menotti M, Liscidini M. Optical resonators based on Bloch surface waves. *Journal of the Optical Society of America B* 2015; 32: 431-438.

[37] Dubey R, Vosoughi Lahijani B, Barakat E, Häyrinen M, Roussey M, Kuittinen M, and Herzig HP. Near-field characterization of a Bloch-surface-wave-based 2D disk resonator. *Optics Letters* 2016; 41, 4867-4870.

[38] Wang R, Wang Y, Zhang D, Si G, Zhu L, Du L, Kou S, Badugu R, Rosenfeld M, Lin J, Wang P, Ming H, Yuan X, Lakowicz JR. Diffraction-Free Bloch Surface Waves. *ACS Nano* 2017; 11(6): 5383-5390.

[39] Kovalevich T, Belharet D, Robert L, Kim MS, Herzig HP, Grosjean T, Bernal MP. Experimental evidence of Bloch surface waves on photonic crystals with thin-film LiNbO3 as a top layer. *Photonics Research* 2017; 5(6): 649-653.

[40] Wang R, Xia H, Zhang D, Chen J, Zhu L, Wang Y, Yang E, Zang T, Wen X, Zou G, Wang P, Ming H, Badugu R, Lakowicz JR. Bloch surface waves confined in one dimension with a single polymeric nanofiber. *Nature Communication* 2017; 8: 14330.

[41] Baghbadorani HK, Aurelio D, Barvestani J, Liscidini M. Guided modes in photonic crystal slabs supporting Bloch surface waves. *J. Opt. Soc. Am. B* 2018; 35: 805-810.

[42] Wang M, Zhang H, Kovalevich T, Salut R, Kim MS, Suarez MA, Bernal M, Herzig HP, Lu H, Grosjean T. Magnetic spin-orbit interaction of light. *Light-Science & Applications* 2018; 7:24.

[43] Kim MS, Vetter A, Rockstuhl C, Lahijani BV, Häyrinen M, Kuittien M, Roussey M, Herzig HP. Multiple self-healing Bloch surface wave beams generated by a two-dimensional fraxicon. *Communications Physics* 2018; 1:63.

[44] Vosoughi Lahijani B, Badri Ghavifekr H, Dubey R, Kim MS, Vartiainen I, Roussey M, Herzig HP. Experimental demonstration of critical coupling of whispering gallery mode cavities on a Bloch surface wave platform. *Optics. Letters* 2017; 42:5137-5140.

[45] Aurelio D, Liscidini M. Electromagnetic field enhancement in Bloch surface waves. *Physical Review B* 2017; 96: 045308.

[46] Liscidini M, Galli M, Shi M, Dacarro G, Patrini M, Bajoni D, Sipe JE. Strong modification of light emission from a dye monolayer via Bloch surface waves. *Optics Letters* 2009; 34: 2318-2320.

[47] Ballarini M, Frascella F, Michelotti F, Digregorio G, Rivolo P, Paeder V, Musi V, Giorgis F, Descrovi E. Bloch surface waves-controlled emission of organic dyes grafted on a one-dimensional photonic crystal. *Applied Physics Letters* 2011; 99: 043302.

[48] Badugu R, Nowazcyk K, Descrovi E, Lakowicz JR. Radiative decay engineering 6: fluorescence on one-dimensional photonic crystals. *Analytical Biochemistry* 2013; 442: 83-96.

[49] Pirotta S, Patrini M, Liscidini M, Galli M, Dacarro G, Canazza G, Guizzetti G, Comoretto D, Bajoni D. Strong coupling between excitons in organic semiconductors and Bloch surface waves. *Applied Physics Letters* 2014; 104:51111.

[50] Ray K, Badugu R. Lakowicz JR. Bloch Surface Wave-Coupled Emission from Quantum Dots by Ensemble and Single Molecule Spectroscopy. *RSC advances* 2015; 5(67):54403-54411.

[51] Romodina MN, Soboleva IV, Fedyanin AA. Magneto-optical switching of Bloch surface waves in magnetophotonic crystals. *Journal of Magnetism and Magnetic Materials* 2016; 415:82-86.

[52] Lerario G, Ballarini D, Fieramosca A, Cannavale A, Genco A, Mangione F, Gambino S, Dominici L, De Giorgi M, Gigli G, Sanvitto D. High-speed flow of interacting organic polaritons. *Light: Science & Applications* 2017; 6: e16212.

[53] Lerario G, Ballarini D, Dominici L, Fieramosca A, Cannavale A, Holwill M, Kozikov A, Novoselov KS, Gigli G. Bloch Surface Waves for MoS_2 Emission Coupling and Polariton Systems. *Applied Sciences* 2017; 7:1217.

[54] Toma K, Descrovi E, Toma M, Ballarini M, Mandracci P, Giorgis F, Mateescu A, Jonas U, Knoll W, Dostálek J. Bloch surface wave-enhanced fluorescence biosensor. *Biosensors and Bioelectronics* 2013; 43(1):108-114.

[55] Frascella F, Ricciardi S, Pasquardini L, Potrich C, Angelini A, Chiadò A, Pederzolli C, De Leo N, Rivolo P, Pirri CF, Descrovi E. Enhanced fluorescence detection of miRNA-16 on a photonic crystal. *Analyst* 2015; 140(16):5459-5463.

[56] Angelini A, Barakat E, Munzert P, Boarino L, De Leo N, Enrico E, Giorgis F, Herzig HP, Pirri CF, Descrovi E. Focusing and extraction of light mediated by Bloch surface waves. *Scientific Reports* 2014; 4: 5428.

[57] Yu L, Barakat E, Sfez T, Hvozdara L, Di Francesco J, Herzig HP. Manipulating Bloch surface waves in 2D: a platform concept-based flat lens. *Light-Science & Applications* 2014; 3: e124.

[58] Lahijani BV, Descharmes N, Osowiecki G, Barbey R, Herzig HP. Bloch surface waves Fabry-Pérot Nanocavity, *Journal of Physics: Conference Series* 2018; 1092:012163.

[59] Descrovi E, Giorgis F, Dominici L, Michelotti F. Experimental observation of optical bandgaps for surface electromagnetic waves in a periodically corrugated one-dimensional silicon nitride photonic crystal. *Opt. Lett.* 2008; 33: 243-245.

[60] Pitanti A, Ghulinyan M, Navarro-Urrios D, Pucker G, Pavesi L. Probing the spontaneous emission dynamics in Si-nanocrystals-based microdisk resonators. *Physical Review Letters* 2010; 104: 103901.

[61] Angelini A, Munzert P, Enrico E, De Leo N, Scaltrito L, Boarino L, Giorgis F, Descrovi E. Surface-Wave-Assisted Beaming of Light Radiation from Localized Sources. *ACS Photonics* 2014; 1(7): 612–617.

[62] Tran TT, Kianinia M, Bray K, Kim S, Xu ZQ, Gentle A, Sontheimer B, Bradac C, Aharonovich I. Nanodiamonds with photostable, sub-gigahertz linewidth quantum emitters. *APL Photonics* 2017, 2(11): 116103.

[63] Grosso G, Moon H, Lienhard B, Ali S, Efetov D.K, Furchi, MM, Jarillo-Herrero P, Ford MJ, Aharonovich I, Englund D. Tunable and high-purity room temperature single-photon emission from atomic defects in hexagonal boron nitride. *Nature Communications* 2017; 8(1):705.